



SADDLE AND NODAL POINT IMPACT ON MAGNETOHYDRODYNAMIC STAGNATION-POINT FLOW OF CASSON NANOFUID FLOW TOWARD HOWARTH'S WAVY CIRCULAR CYLINDER

G. Kathyayani^{1*}, P Venkata Subrahmanyam²

^{1*}Department of Applied Mathematics, Yogi Vemana University, Kadapa, A.P., India, Email: kathyagk@yvu.edu.in

²Department of Applied Mathematics, Yogi Vemana University, Kadapa, A.P., India, Email: pvsmsubbu@gmail.com

Abstract:

Casson fluid flow helps us understand and model fluids that do not follow Newton's law of viscosity. Many real-world fluids, such as blood, ketchup, paints, and various biological fluids, exhibit non-Newtonian behaviour. The present exploration presents the numerical investigation of a Casson nanofluid flow's MHD stagnation-point flow over Howarth's wavy circular cylinder. The coupled nonlinear ODE is generated from a nonlinear partial differential equation with the use of similarity transformations. After that, the MATLAB software's built-in *bvp4c* is used for the numerical solution of the nonlinear system. The pertinent governing parameters impact on temperature, velocity and concentration profiles are examined through graphs. Numerical values of physical quantities such as friction coefficient in x and y directions, diffusion mass flux, and local Nusselt number are employed. The influence of Casson parameter stabilizes the momentum boundary layer growth on axial velocity and radial velocity profiles and reduced the thermal and concentration boundary layer.

Keywords: Casson nanofluid, 3D stagnation-point flow, saddle/nodal points, wavy cylinder, magnetohydrodynamics.

NOMENCLATURE

E_a	Activation energy	Sc	Schmidt number
E	Activation energy parameter	C_p	Specific heat
D_B	Brownian diffusion coefficient, kg/m s	Greek symbols	
Nb	Brownian motion parameter	β	coefficient of thermal expansion
x, y, z	Cartesian coordinates	ν	kinematic viscosity
a, b, c	Constants	θ	Dimensionless temperature
f, g	Dimensionless stream profiles	σ	Electric conductivity
Ec_x, Ec_y	Eckert numbers	ρ	fluid density
T	Fluid temperature	α	thermal diffusivity
u_e, v_e, w_e	Free stream velocities	η	Similarity variable
Le	Lewis number	ϕ	Nanoparticle volume fraction
M	Magnetic parameter	Subscripts	
C	Nanoparticle concentration	w	Conditions on the wall
Pr	Prandtl number	∞	ambient condition

1. Introduction

Nanofluid behavior is studied using the two-phase nanofluid model, which is a computational and mathematical framework for studying liquid suspensions containing nanoparticles. In comparison with traditional fluids, nanofluids have superior thermal and electrical properties. As a result, they are particularly useful for heat transfer and cooling systems in various engineering applications. Flow of Casson fluid is the motion of a fluid that does not follow Newtonian laws, which is a rheological model of fluid flow describing the relationship between shear stress and shear rate. When compared to Newtonian fluids, which have a direct correlation between the rate of shear with shear stress, non-Newtonian fluids, such as Casson fluid, behave differently. Newtonian fluids (such as water and air) have linear behavior.

Casson fluid flow helps us understand and model fluids that do not follow Newton's law of viscosity. Many real-world fluids, such as blood, ketchup, paints, and various biological fluids, exhibit non-Newtonian behavior. Understanding the flow of these materials is crucial for many industrial, medical, and biological applications. It can also be used to model blood flow through vessels at high shear rates Shaw et al. (2009). It has been widely used in engineering science simulation to simulate Casson's rheological behaviour in energy and industrial systems using various analytical and computational methods. By using a model that accounts for Brownian motion as well as thermophoresis and convective nanofluid transport, Buongiorno (2006) conducted a comprehensive investigation into convective transport in nanofluids. It was Buongiorno (2006) who proposed an equilibrium model for the momentum, heat transfer and mass in nanofluids that includes two components, four equations, and is non-homogeneous. With the help of a Brownian motion and thermophoresis model, Buongiorno (2006) surveyed convective transport in nanofluids. Ibrahim et al. (2017) presented the influence of viscous dissipation on chemically reactive Casson's MHD nanofluid flow over a stretching surface using the Casson nanofluid as a model. Using Brownian motion, thermophoresis, and non-linear thermal radiation, Venkata Ramudu et al. (2020) explored the convective boundary conditions of the electrically conducting Casson nanofluid's flow across a stretching surface. Under time-dependent velocity, zero mass flux boundary conditions, and temperature of the convective wall, Thumma et al. (2019) present numerically three-dimensional unsteady Casson nanofluid towards an impermeable stretchable sheet when viscous dissipation, thermal radiation and heat generation are involved. A convectively heated stretching sheet with a thermally radiating and dissipative magnetohydrodynamic Casson nanofluid flow liquid is investigated by Kumar et al. (2021) under Joule heating effect. They found that Casson nano liquids have plastic dynamic viscosity, which reduces entropy generation rate. Faisal et al. (2020) deliberated a boundary layer flow of Casson nanomaterial triggered by an unsteady moveable surface is analyzed, considering the significance of the magnetic field, porous space, and prescribed surface temperature. According to Tulu et al. (2020), the Casson nanofluid flow toward a stretched cylinder with variable thermal conductivity is modeled using the Cattaneo-Christov heat flux model. They observed that, compared to Cattaneo-Christov heat flux, Fourier's law of heat conduction has a lower local heat transfer rate. Using the two-phase nanofluid model in bioconvective Casson fluid with hybrid nanoparticles, Lone et al. (2023) studied the behaviour of heat and mass transfer across an exponential sheet. Chu et al. (2023) discussed Fourier and Fick's generalized laws can be applied to analyze the stagnation point flow of a micropolar fluid over a stretching surface in presence of activation energy, thermophoretic, and radiation effects within magnetized viscoelastic liquids. There has been a debate between investigators regarding the study's several physical parameters and the features of mass and heat distribution in Newtonian as well as non-Newtonian fluids (Mirza Naveed et al., 2023, Vijay et al., 2023, Khan et al., 2023, Makhdom et al., 2023, Devi et al., 2020, Venkatadri et al., 2018, 2023). Thereafter, multiple numerical studies were carried out extensively by Wakif et al. (2022, 2023), Elboughdiri et al. (2023), Ghernaout et al. (2023), Zhang et al. (2023), Sharma et al. (2023), Shakif et al. (2023), Rasool et al. (2023), Hameed et al. (2022), Shah et al. (2022), Tawade et al. (2022), Khan et al. (2022) and Shabnam et al. (2022).

Hydromagnetic Casson nanofluid flow past a circular sinusoidal cylinder in combination with an adapted Buongiorno nanofluid model had not been investigated yet, based on a literature review. By addressing this gap, this work aims to fill it. This research work further advances the real-world application of this research by deploying experimentally derived functions of effective dynamic viscosity and effective thermal conductivity. Major works has been studied on different nanofluids past a stretching cylinder with various external thermal forces. The reasons mentioned above motivated us to accomplish the present study. In the present manuscript, the numerical investigating an MHD stagnation-point flow of a Casson nanofluid flow over a circular sinusoidal cylinder that has a steady three-dimensional incompressible flow with viscous dissipation and activation energy has been addressed. With the help of a two-phase nanofluid model, a steady flow of non-Newtonian Casson

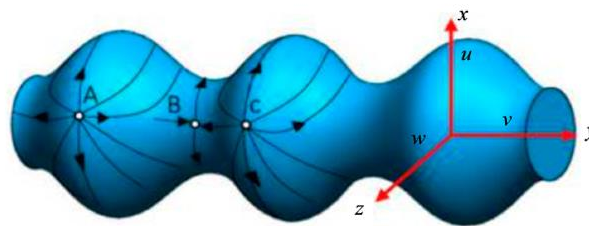
nanofluids is investigated. The current study's main objective and novelty is to examine the impacts of viscous dissipation and Arrhenius energy on MHD Casson nanofluid flow toward Howarth's circular wavy cylinder. The graphical representation has been exhibited with the influence of Nb, Nt, M, c and Sc of Boundary layer flow at stagnation-point nanofluid flow past a 3-D Sinusoidal Cylinder.

2. Mathematical Formulation

A steady stagnation-point flow incompressible Casson nanofluid is considered to towards a wavy cylinder (Fig. 1). Throughout the radius of the cylinder, there are points of stagnation (points A, B, and C) at each extreme of the radius. Streamlines can be described by the equation $x = \delta y^c$, where c is the fraction of the slope of the stream velocities and expressed as $c = \frac{b}{a}$ is called nodal point with $0 < c < 1$, or saddle point with $-1 < c < 0$ and finally $c=0$ refers for plane flow, δ is constant, which gives a particular streamline. In the cylinder, the points of minimum and maximum stagnation can be seen at positions B, A, and C. The fluid flow particles velocity profiles in the direction of x, y, and z is considered with u, v, and w, respectively. It is significant to note that the stagnation point in the Cartesian coordinate system Oxyz lies at the origin of the system and velocity profiles are taken at the form:

$$u_e = ax, \quad v_e = aby, \quad w_e = -(a+b)z$$

(a)



Nodal attachment points (A and C)

Saddle Attachment Point (B)

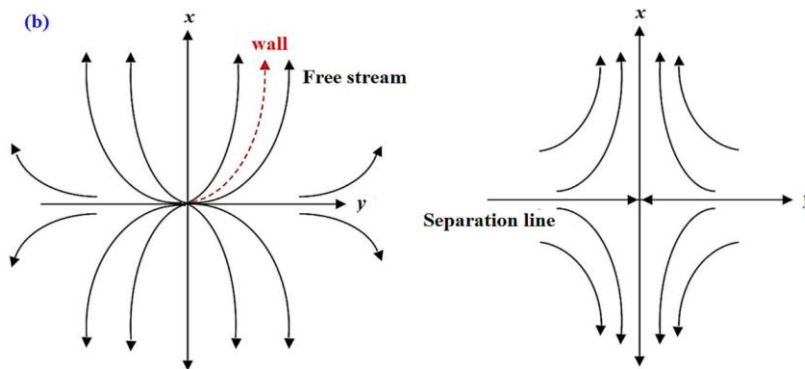


Fig. 1: Schematic model and the streamlines

In the stress-strain relation, the constitutive equation for a Casson fluid is as follows (Devi *et al.*(2020), Venkatadri *et al.*(2023), Pramanik *et al.*(2014)):

$$\tau^{\frac{1}{2}} = \tau_0^{\frac{1}{2}} + \mu \gamma^{\frac{1}{2}}$$

$$\tau_{ij} = \begin{cases} 2(\mu_B + \frac{P_y}{\sqrt{2\pi}})e_{ij}, & \pi > \pi_c \\ 2(\mu_B + \frac{P_y}{\sqrt{2\pi_c}})e_{ij}, & \pi_c > \pi \end{cases} \tag{1}$$

A sinusoidal cylinder's boundary layer can be modelled by applying the equations shown below to represent the boundary layer over the cylinder in accordance with the assumptions suggested above, and after removing the pressure using the Bernoulli equation, in order to model the boundary layer over the sinusoidal cylinder with incorporating the Casson rheological effect term from Eqn. (1) (Raju *et al.*, 2023, Raizah *et al.*, 2023, Kathyayani *et al.*, 2019).

$$\frac{\partial u}{\partial x} + \frac{\partial v}{\partial y} + \frac{\partial w}{\partial z} = 0 \tag{2}$$

$$u \frac{\partial u}{\partial x} + v \frac{\partial u}{\partial y} + w \frac{\partial u}{\partial z} = a^2 x + \nu \left(1 + \frac{1}{\beta} \right) \frac{\partial^2 u}{\partial z^2} - \frac{\sigma B_0^2}{\rho} (u - ax) \tag{3}$$

$$u \frac{\partial v}{\partial x} + v \frac{\partial v}{\partial y} + w \frac{\partial v}{\partial z} = b^2 y + \nu \left(1 + \frac{1}{\beta} \right) \frac{\partial^2 v}{\partial z^2} - \frac{\sigma B_0^2}{\rho} (v - by) \tag{4}$$

$$u \frac{\partial T}{\partial x} + v \frac{\partial T}{\partial y} + w \frac{\partial T}{\partial z} = \alpha \frac{\partial^2 T}{\partial z^2} + \tau \left[D_B \frac{\partial T}{\partial z} \frac{\partial C}{\partial z} + \frac{D_T}{T_\infty} \left(\frac{\partial T}{\partial z} \right)^2 \right] + \frac{\mu}{\rho c_p} \left(1 + \frac{1}{\beta} \right) \left[\left(\frac{\partial u}{\partial z} \right)^2 + \left(\frac{\partial v}{\partial z} \right)^2 \right] \tag{5}$$

$$u \frac{\partial C}{\partial x} + v \frac{\partial C}{\partial y} + w \frac{\partial C}{\partial z} = D_m \frac{\partial^2 C}{\partial z^2} + \frac{D_T}{T_\infty} \frac{\partial^2 T}{\partial z^2} - K_r \left(\frac{T}{T_\infty} \right)^n e^{-\frac{E_a}{K_r T}} (C - C_\infty) \tag{6}$$

As a result of these boundary conditions, the formula is as follows:

$$u = v = w = 0, T = T_w, C = C_w \quad \text{at} \quad z = 0 \tag{7}$$

$$u \rightarrow u_e, v \rightarrow v_e, T \rightarrow T_\infty, C \rightarrow C_\infty \quad \text{as} \quad z \rightarrow \infty$$

There is a similarity solution to each equation of the form

$$u = axf'(\eta), v = byg'(\eta), w = -\sqrt{av}(f(\eta) + cg(\eta)), \frac{T - T_\infty}{T_w - T_\infty} = \theta(\eta) \tag{8}$$

$$\phi(\eta) = \frac{C - C_\infty}{C_w - C_\infty}, \eta = z\sqrt{\frac{a}{\nu}}$$

It is worth noting that derivative with respect to η denotes the primes. The differential equations (2)-(6) reduced to ODEs, which are nonlinear in nature, with the help of similarity transformations (8).

$$\left(1 + \frac{1}{\beta} \right) f''' + (f + cg) f'' - (f')^2 + 1 - M(f' - 1) = 0 \tag{9}$$

$$\left(1 + \frac{1}{\beta} \right) g''' + (f + cg) g'' - c(g')^2 + c - M(g' - 1) = 0 \tag{10}$$

$$\frac{1}{Pr} \theta'' + (f + cg) \theta' + Nb \theta' \phi' + Nt(\theta')^2 + \left(1 + \frac{1}{\beta} \right) Ec_y (Ec_m f''^2 + g''^2) = 0 \tag{11}$$

$$\phi'' + Sc(f + g) \phi' + \frac{Nt}{Nb} \theta'' - Sc \sigma (1 + \delta \theta)^n \exp\left(\frac{-E}{1 + \delta \theta}\right) \phi = 0 \tag{12}$$

The modified boundary conditions are

$$\begin{aligned}
 f = 0, f' = 0, g = 0, g' = 0, \theta = 1, \phi = 1 & \quad \text{at} \quad \eta = 0 \\
 f' = 0, g' = 0, \theta = 0, \phi = 0 & \quad \text{at} \quad \eta = \infty
 \end{aligned}
 \tag{13}$$

Eckert numbers $Ec_x = \frac{a^2 x^2}{c_p (T_w - T_\infty)}$, $Ec_y = \frac{b^2 y^2}{c_p (T_w - T_\infty)}$, Thermophoresis $Nt = \frac{D_T (T_w - T_\infty)}{\nu T_\infty}$, Brownian motion $Nb = \frac{D_B (T_w - T_\infty)}{\nu}$, Prandtl number $Pr = \frac{\nu}{\alpha}$, Magnetic field $M = \frac{\sigma B_0^2}{a \rho}$, Schmid number $Sc = \frac{\nu}{D_m}$.

Modified Eckert number $Ec_m = \frac{Ec_x}{Ec_y}$. The interested quantities are friction coefficients in the x and y directions

are correlated by two physical quantities, C_{f_x} and C_{f_y} , the local Nusselt and Sherwood numbers, which are defined by:

$$C_{f_x} = \frac{\tau_{wx}}{\rho \nu_e^2}, \quad C_{f_y} = \frac{\tau_{wy}}{\rho \nu_e^2}, \quad Nu_x = \frac{x q_w}{k (T_w - T_\infty)}, \quad Sh_x = \frac{x s_w}{D_B (C_w - C_\infty)}
 \tag{14}$$

Where $\tau_{wx} = \mu \left(1 + \frac{1}{\beta} \right) \frac{\partial u}{\partial z} \Big|_{z=0}$ and $\tau_{wy} = \mu \left(1 + \frac{1}{\beta} \right) \frac{\partial v}{\partial z} \Big|_{z=0}$ are the surface shear stress along the x and y directions, respectively, $q_w = -k \frac{\partial T}{\partial z} \Big|_{z=0}$ is the surface heat flux, and $s_w = -D_B \frac{\partial C}{\partial z} \Big|_{z=0}$ is the surface mass flux.

Using Eq. (8), we obtain

$$\begin{aligned}
 [Re_x]^{\frac{1}{2}} C_{f_x} &= \left(1 + \frac{1}{\beta} \right) f''(0), \quad \left(\frac{x}{y} \right) C_{f_y} [Re_x]^{\frac{1}{2}} = c \left(1 + \frac{1}{\beta} \right) g''(0), \\
 [Re_x]^{\frac{-1}{2}} Nu_x &= -\theta'(0), \quad [Re_x]^{\frac{-1}{2}} Sh_x = -\phi'(0), \quad Re_x = \frac{u_e x}{\nu}
 \end{aligned}
 \tag{15}$$

3. Method of Solution

In this computational section, we combine the shooting scheme with Runge-Kutta method to solve the coupled nonlinear ODEs (9) to (12) of Magnetohydrodynamic (MHD) stagnation-point nanofluid flow past a 3-D Sinusoidal Cylinder with boundary conditions (13). we are considered for [0,15] as the domain of the boundary value problem in terms of [0, ∞). Interestingly, the results are unaffected after $\eta = 15$ in computational Runge-Kutta method with the shooting scheme. In order for the computation method to work, the governing nonlinear ODEs (9) to (12) must be converted into system of first-order ODEs.

The first-order ODE system is defined as follows:

$$\begin{aligned}
 f &= y_1, f' = y_2, f'' = y_3, f''' = y_3' \\
 g &= y_4, g' = y_5, g'' = y_6, g''' = y_6' \\
 \theta &= y_7, \theta' = y_8, \theta'' = y_8' \\
 \phi &= y_9, \phi' = y_{10}, \phi'' = y_{10}'
 \end{aligned}$$

Thus, the simultaneous systems of first-order ODEs are as follows:

$$\begin{aligned}
 y_1' &= y_2, \\
 y_2' &= y_3, \\
 y_3' &= -\left(c y_3 y_4 + y_1 y_3 - y_2^2 + 1 - M (y_2 - 1) \right) / \left(1 + \frac{1}{\beta} \right)
 \end{aligned}$$

$$y_4' = y_5,$$

$$y_5' = y_6,$$

$$y_6' = -\left(cy_6y_4 + y_1y_6 - cy_5^2 + c - M(y_5 - 1)\right) / \left(1 + \frac{1}{\beta}\right),$$

$$y_7' = y_8,$$

$$y_8' = -Pr \left(y_8y_1 + cy_8y_4 + Nty_8^2 + Nby_8y_{10} + \left(1 + \frac{1}{\beta}\right) \left(Ec_x(y_3^2) + Ec_y(y_6^2) \right) \right)$$

$$y_9' = y_{10},$$

$$y_{10}' = -\left(Sc(y_{10}y_1 + cy_{10}y_4) + \frac{Nt}{Nb} y_8' - Sc \sigma (1 + \delta y_7)^n \exp\left(\frac{-E}{1 + \delta y_7}\right) y_9 \right)$$

$$y_1(0) = 0, y_2(0) = 0, y_3(0) = p_0, y_4(0) = 0, y_5(0) = 0,$$

$$y_6(0) = p_1, y_7(0) = 1, y_8(0) = p_2, y_9(0) = 1, y_{10}(0) = p_3.$$

The unknown initial estimates P_0, P_1, P_2 and P_3 are computed by Newton-Raphson method with convergence tolerance to $\varepsilon = 10^{-9}$.

We have computed numerical results for local Nusselt number, local Sherwood number, and dimensionless friction coefficients for a steady flow that excludes thermophoresis or Brownian motion effects. Upon comparing our results with past research, we discovered a remarkable agreement to the findings reported by Dinarvand *et al.* (2013). You can find a summary of our discoveries in Table 1, Which also provides good confidence for further findings using this present numerical method.

4. Results and Discussion

This section demonstrates the numerically computed graphical outcomes and thermo-physical description of relevant terms over the nanofluid velocity profiles in x and y directions, temperature profile, nanofluid concentration profile and physical quantities. The numerical investigating an MHD Casson nanofluid flow’s stagnation-point over a circular sinusoidal cylinder that has a steady three-dimensional incompressible flow with viscous dissipation and activation energy has been addressed. With the help of a two-phase nanofluid model, a steady flow of non-Newtonian Casson nanofluids is investigated. The results of several parameters on the coefficient of skin friction, the local Sherwood number and the local Nusselt number together with the velocity, concentration, and temperature are provided by Figures 2–10 in graphical form and Tables 1-3 in tabular form. The impacts of various parameters are addressed in detail. In reality, this present work validates the existence of Casson nano fluid solutions for a certain range of controlling parameters.

Table 1: Comparison of friction coefficients, local Sherwood number and local Nusselt number, $c = 0.5$

Source of data	$[Re_x]^{-\frac{1}{2}} C_{f_x}$	$[Re_x]^{-\frac{1}{2}} C_{f_y}$	$[Re_x]^{-\frac{1}{2}} Nu_x$	$[Re_x]^{-\frac{1}{2}} Sh_x$
Dinarvand <i>et al.</i> (2013)	1.2680	0.4991	1.3303	-----
Present work	1.2678	0.4991	1.3302	0.7063
Error %	0.015	0	0.0075	-----

Table 2: Numerical results of local skin friction.

M	β	Pr	Ec_y	$[Re_x]^{1/2} C_{fx}$			$[Re_x]^{1/2} C_{fy}$		
				c = -0.5	c = 0	c = 0.5	c = -0.5	c = 0	c = 0.5
0.5	0.2	6.2	0.01	3.445733	3.477695	3.551675	0.949427	2.142997	2.977617
0				3.013334	3.019211	3.103175	-0.272736	1.397349	2.444863
1				3.842563	3.883251	3.949871	1.803803	2.724665	3.434560
3				5.159584	5.200856	5.250573	3.841007	4.381067	4.864790
7				7.110439	7.143354	7.179197	6.213696	6.564440	6.898374
	0.2			3.445733	3.477695	3.551675	0.949427	2.142997	2.977617
	0.4			2.631724	2.656133	2.712637	0.725071	1.636741	2.274192
	0.8			2.110074	2.129644	2.174948	0.581351	1.312312	1.823410
	∞			1.406716	1.419763	1.449965	0.387567	0.874875	1.215607

Table 3: Numerical outcomes of $[Re_x]^{-1} Nu_x$

M	β	Pr	Nb	Nt	Ec_m	Ec_y	$[Re_x]^{-1} Nu_x$		
							c = -0.5	c = 0	c = 0.5
0.5	0.2	6.2	0.6	0.2	1	0.01	0.255279	0.244024	0.262020
0							0.268019	0.247295	0.260031
1							0.241034	0.239856	0.262116
3							0.194458	0.220695	0.254470
7							0.127207	0.181159	0.227925
	0.2						0.255279	0.244024	0.262020
	0.4						0.289610	0.278035	0.300429
	0.8						0.320567	0.307737	0.334000
	∞						0.383505	0.366747	0.401279
		3					0.306952	0.309318	0.342449
		5					0.255279	0.244024	0.262020
		7					0.199015	0.178311	0.184471
		9					0.147111	0.120381	0.118135
			0.2				0.459612	0.465697	0.518837
			0.4				0.348536	0.344149	0.377026
			0.6				0.255279	0.244024	0.262020
			0.8				0.179302	0.164278	0.172066
				0.2			0.255279	0.244024	0.262020
				0.4			0.192673	0.178038	0.187868
				0.6			0.143046	0.126756	0.131046
				0.8			0.104223	0.087463	0.088115
					1		0.255279	0.244024	0.262020
					2		0.212024	0.202545	0.222809
					3		0.168714	0.161015	0.183551
					4		0.125350	0.119434	0.144247
						0.0	0.304689	0.305178	0.331059
						0.01	0.255279	0.244024	0.262020
						0.03	0.156165	0.121301	0.123457
						0.05	0.056662	-0.001971	-0.015748

The display of the axial velocity and radial velocity profile vs β is shown in Fig. 2(a)–(b), while maintaining $c = -0.5$ (dashes) and $c = 0.5$ (solid line). Both velocities enhanced with raising values of β . Figure 3(a) and (b) reveal how energy and concentration profiles change in response to variations in β , the noddle point, while maintaining $c = -0.5$ (dashes) and $c = 0.5$ (solid line). These figures demonstrate that as β increases, both the energy and concentration profiles exhibit a decrease. The behavior of the boundary layer of axial velocity and

radial velocity profile against M is depicted by Figures 4(a)–(b), while maintaining $c = 0.5$ and $c = -0.5$, respectively. It is clear that the greater impact on the velocity profiles is noted with rising M. Mainly magnetic field stimulates the fluid particles which enhances the velocities of these particles.

Table 4: Numerical outcomes of local Sherwood number $[\text{Re}_x]^{-1} Sh_x$

M	β	Pr	Sc	E	σ	$[\text{Re}_x]^{-1} Sh_x$		
						$c = -0.5$	$c = 0$	$c = 0.5$
0.5	0.2	6.2	0.5	0.5	0.2	0.228822	0.285146	0.365073
0						0.252104	0.268581	0.346297
1						0.218583	0.298715	0.380205
3						0.221983	0.337370	0.422726
7						0.252738	0.384631	0.473990
	0.2					0.243658	0.309529	0.394936
	0.4					0.248957	0.320843	0.409249
	0.8					0.251447	0.327520	0.417859
	∞					0.254318	0.354530	0.454293
		3				0.208956	0.260886	0.335601
		5				0.228822	0.285146	0.365073
		7				0.248775	0.308119	0.392001
		9				0.266703	0.327944	0.414587
			0.3			0.163335	0.215292	0.279619
			0.5			0.228822	0.285146	0.365073
			0.7			0.271237	0.331158	0.422546
			0.9			0.301697	0.364793	0.465509
				0.5		0.228822	0.285146	0.365073
				1.0		0.268998	0.319322	0.393171
				1.5		0.294158	0.341139	0.411399
				2.0		0.310409	0.355402	0.423434
					0.0	0.343237	0.384736	0.448493
					0.1	0.288675	0.336726	0.407853
					0.2	0.228822	0.285146	0.365073
					0.3	0.162476	0.229392	0.319899

Fig. 5(a-b) depict the impact of M on temperature and concentration profiles, accordingly, while maintaining c at -0.5 (dishes) and c at 0.5 (solid line), respectively. It is clear from the data that when the value of M rises, it enhances the resistance of temperature profiles against $c = -0.5$. However, we observe a contrasting behavior when $c = 0.5$, shown in Fig. 5(a). Figure 5(b) establish the distribution of concentration profiles with different controlling parameter M, while maintaining $c = -0.5$ (dashes) and $c = 0.5$ (solid line), respectively. The results indicate that the value of M increases, it is confirmed to enhance the resistance of concentration profiles when $c = -0.5$; however, an opposing trend is observed with $c = 0.5$, as depicted in Fig. 5(b). The effect of Thermophoresis parameter on temperature distribution and concentration profile is shown in Fig. 6(a-b), while maintaining $c = 0.5$ and $c = -0.5$. The temperature and concentration profile improve as the Thermophoresis parameter's value increases. This suggests that the presence of nanoparticles results in an increased the hydrodynamic boundary layer's thickness under the given conditions. Furthermore, the thermal conductivity is enhanced, leading to a rise in the thermal boundary layer thickness as the volume fraction of nanoparticle increases. The figure, labeled Fig. 7(a-b), illustrates the impact of Nb on the distribution of concentration and temperature profiles. In this experiment, the value of c was set to -0.5 (shown as dashed lines) and 0.5 (represented by solid lines). As Nb increases, the temperature profile shows an increase, while the concentration profiles demonstrate a decrease. Additionally, the concentration profiles are further intensified by the thermophoresis parameter. Figure 8(a-b) illustrates how the Schmidt number affects the concentration and temperature profiles. As Schmidt number rises, there is a decrease in concentration. This leads to a decrease in concentration buoyancy effects, resulting in a decrease in fluid velocity. The decrease in concentration and temperature is accompanied by a reduction in the thickness of the concentration and thermal boundary layers. In a thermal boundary layer, this behavior is analogous to increasing the Prandtl number. Therefore, when Sc increases, the concentration drops.

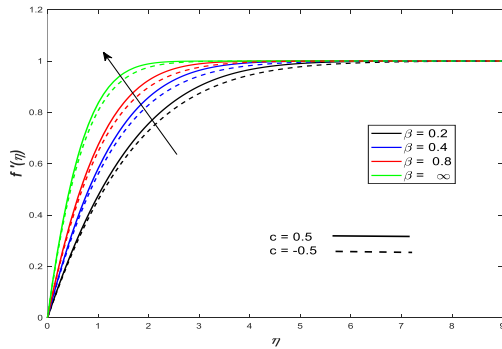


Fig. 2a: Variations in velocity profiles due to β

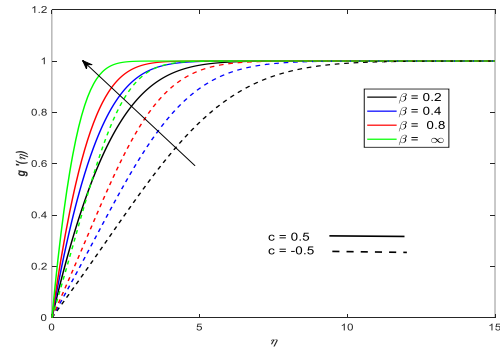


Fig. 2b: Variations in velocity profiles due to β .

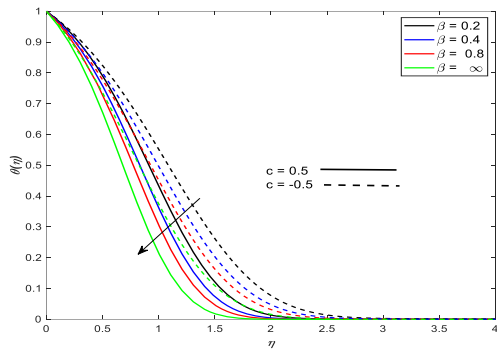


Fig. 3a: Variation in temperature due to β

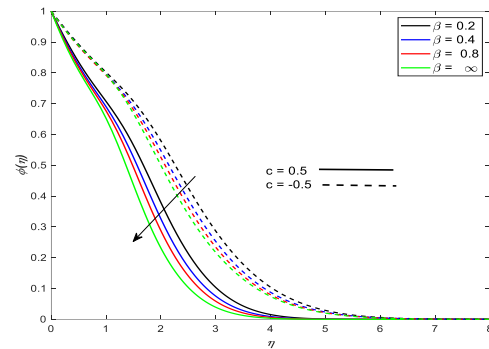


Fig. 3b: Variation in concentration due to β .

Figure 9 (a-b) demonstrates the impact of the Eckert number (Ec) on the concentration and temperature of the fluid. When the value of Ec rises, the fluid temperature rises, as depicted in Figure 9(a). This occurs because heat is generated within the fluid as the Ec value increases, primarily due to the effects of frictional heating. The Eckert number is the ratio of kinetic energy to specific enthalpy difference between the fluid and the wall. So, as Ec increases, more kinetic energy is transformed into internal energy by work done against the viscous fluid stresses. Thus, raising Ec leads to an enhance in temperature. According to Figure 9(b), it is noted that there is a drop in concentration close to the wall, while it increases as we move away from the wall. Based on Figure 10, it can be observed that a rise in the chemical reaction parameter causes a rapid drop in the concentration profile. This is mainly because as the chemical reaction parameter rises, the concentration field decreases due to the increased number of solute molecules performing a chemical reaction. As a result, the solutal boundary layer's thickness is efficiently decreased by a destructive chemical reaction.

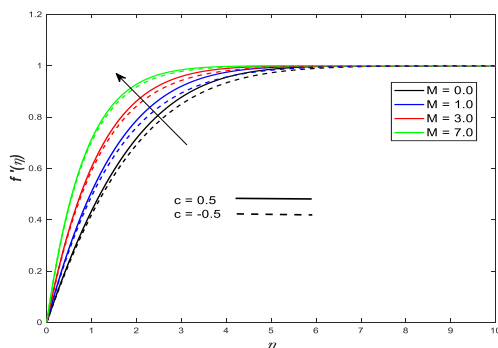


Fig. 4a: Variations in velocity profiles due to M

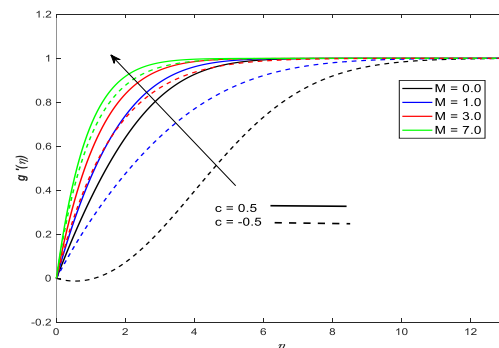


Fig. 4b: Variations in velocity profiles due to M .

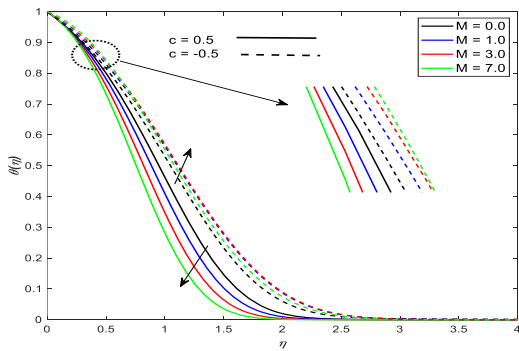


Fig. 5a: Variation in temperature due to M

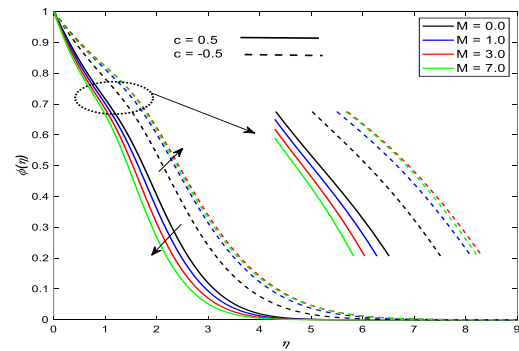


Fig. 5b: Variation in concentration due to M.

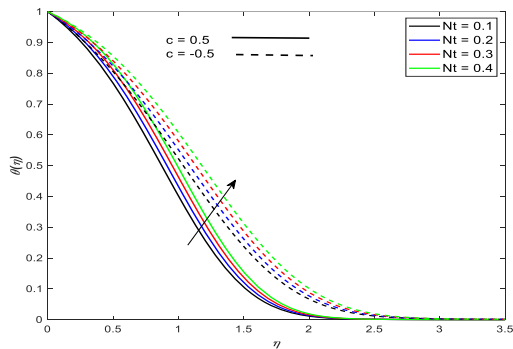


Fig. 6a: Variation in temperature due to Nt

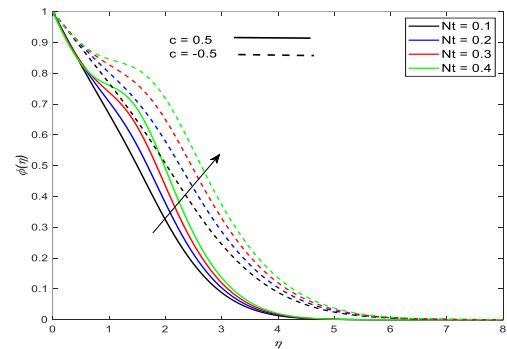


Fig. 6b: Variation in concentration due to Nt

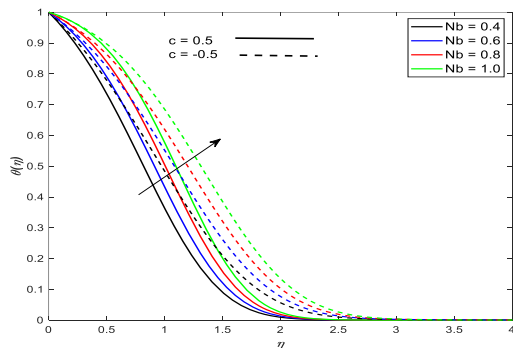


Fig. 7a: Variation in temperature due to Nb.

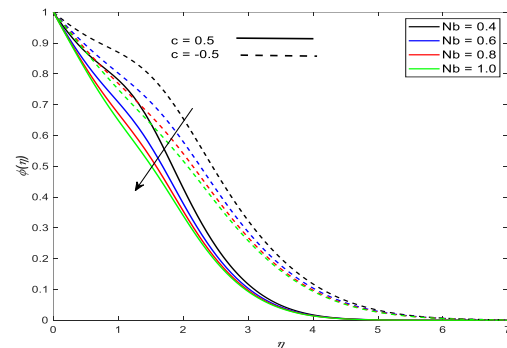


Fig. 7b: Variation in concentration due to Nb.

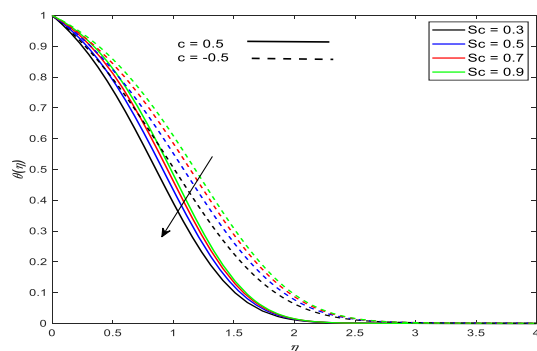


Fig. 8a: Variation in temperature due to Sc

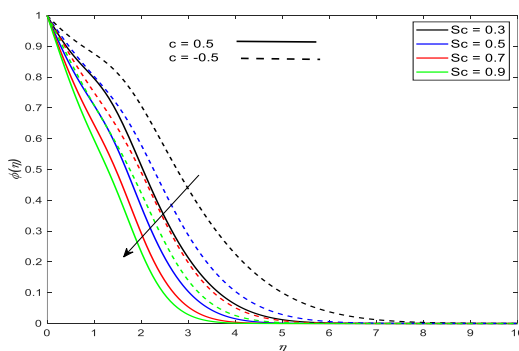


Fig. 8b: Variation in concentration due to Sc

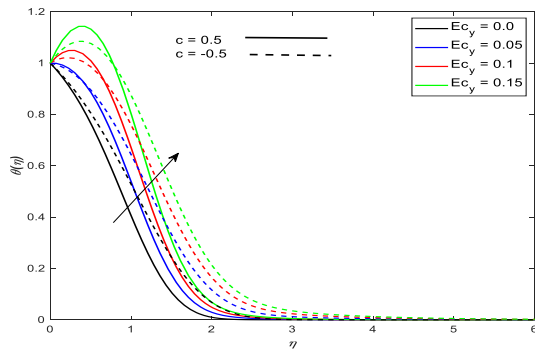


Fig. 9a: Variation in temperature due to Ec_y

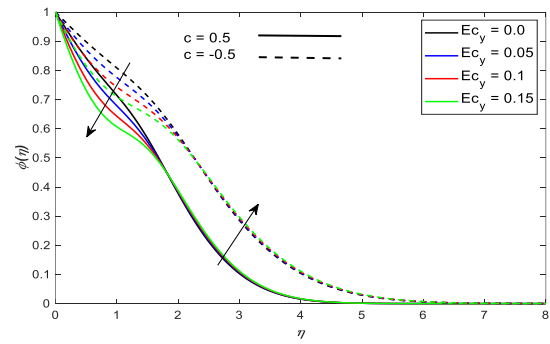


Fig. 9b: Variation in concentration due to Ec_y

From Table 2, we have noticed that the numerical results that the skin friction coefficient increases as the magnetic parameter increases for $C = -0.5, 0, 0.5$ cases while Casson parameter declines the skin friction coefficient. In table-3, we have presented the results for Nusselt number with pertinent parameters $M, \beta, Pr, Nb, Nt, Ec_x$ and Ec_y respectively in three cases $C = -0.5, 0, 0.5$. An enhancing of pertinent parameters $M, \beta, Pr, Nb, Nt, Ec_x$ and Ec_y , the rate of heat transfer is increases with Casson parameter and reduces with M, Pr, Nb, Nt, Ec_x and Ec_y . In table-4, we have presented the results for Sherwood number with pertinent parameters M, β, Pr, Sc, E and σ respectively in three cases $C = -0.5, 0, 0.5$. An enhancing of pertinent parameters $M, \beta, Pr, Nb, Nt, Ec_x$ and Ec_y , the rate of mass transfer increases with β, Pr, E, Sc and reduces with M and σ .

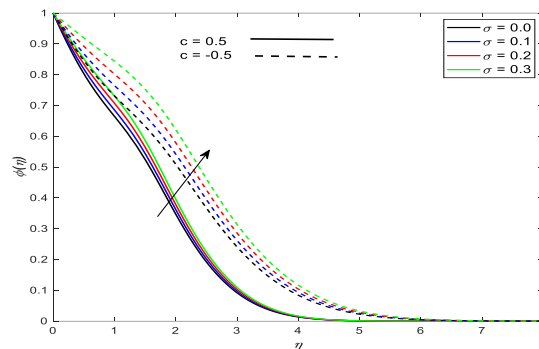


Fig. 10: effect of chemical reaction on concentration profiles

5. Conclusions

In the present manuscript, the numerical investigating an MHD stagnation-point flow of a Casson nanofluid flow over a circular sinusoidal cylinder that has a steady three-dimensional incompressible flow with activation energy and viscous dissipation has been addressed. A steady flow of non-Newtonian Casson nanofluids is explored using a two-phase nanofluid model. From the obtained results, the following conclusions can be deduced.

- The axial velocity and radial velocity profiles at the wall are improved as the magnetic field strength increases.
- The influence of Casson parameter stabilizes the momentum boundary layer growth on axial velocity and radial velocity profiles and reduced the thermal and concentration boundary layer.
- As Thermophoresis parameter increases, the temperature concentration profiles increase rapidly.
- The impact of the Nb shows contrasting effects on the temperature and concentration fields.
- The concentration in the boundary layer is increased by the chemical reaction parameter.
- The performance of heat transmission can be enhanced by 5.95% by adding nanoparticles to the base fluids.

- The introduction of sinusoidal heat at the surface of the cylinder can enhance the phenomenon of maximizing heat transfer over a stretching cylinder near the stagnation point flow.
- The heat transfer enhancement enhances with rising the Brownian motion parameter and decreases the concentration boundary layer.

Declaration of conflicting interests

The author(s) declared no potential conflicts of interest with respect to the research, authorship, and/or publication of this article.

Data availability

The datasets used and/or analyzed during the current study are available from the corresponding author on reasonable request.

Funding

This research received no external funding.

References

- Buongiorno, J. (2006): Convective transport of nanofluids. *J Heat Transfer*, 128: 240- 250. <https://doi.org/10.1115/1.2150834>
- Chu, Y. M., Al-Buriahi, M. S., Khan, A. A., Katub, K. M., Saqlain, M., Abbas, S. Z., and Khan, W. A. (2023): Significance of generalized Fourier and Fick's law and stagnation point flow for magnetized viscoelastic liquids. *Materials Science and Engineering: B*, 296, 116602. <https://doi-org.egateway.vit.ac.in/10.1016/j.mseb.2023.116602>
- Devi, T. S., Lakshmi, C. V., Venkatadri, K., Prasad, V. R., Béq, O. A., and Reddy, M. S. (2020): Simulation of unsteady natural convection flow of a Casson viscoplastic fluid in a square enclosure utilizing a MAC algorithm. *Heat Transfer*, 49(4), 1769-1787. <https://doi.org/10.1002/htj.21690>
- Dinarvand, S, R. Hosseini, E. Damangir, and I. Pop. (2013): Series Solutions for Steady Three-Dimensional Stagnation Point Flow of a Nanofluid Past a Circular Cylinder with Sinusoidal Radius Variation. *Meccanica* 48, 643-652. <https://doi.org/10.1007/s11012-012-9621-7>
- Elboughdiri, N., Reddy, C. S., Alshehri, A., Eldin, S. M., Muhammad, T., and Wakif, A. (2023): A passive control approach for simulating thermally enhanced Jeffery nanofluid flows nearby a sucked impermeable surface subjected to buoyancy and Lorentz forces. *Case Studies in Thermal Engineering*, 47, 103106. <https://doi.org/10.1016/j.csite.2023.103106>
- Faisal, M., Ahmad, I. and Javed, T. (2020): Significances of prescribed heat sources on magneto Casson nanofluid flow due to unsteady bi-directionally stretchable surface in a porous medium. *SN Appl. Sci.* 2, 1472. <https://doi.org/10.1007/s42452-020-03262-4>.
- Ghernaout, D., Elboughdiri, N., Muhammad, T., Alshehri, A., Sadat, R., Ali, M. R., and Wakif, A. (2023) : Towards a novel EMHD dissipative stagnation point flow model for radiating copper-based ethylene glycol nanofluids: An unsteady two-dimensional homogeneous second-grade flow case study. *Case Studies in Thermal Engineering*, 45, 102914. <https://doi.org/10.1016/j.csite.2023.102914>
- Hameed, N., Noeiaghdam, S., Khan, W., Pimpunchat, B., Fernandez-Gamiz, U., Khan, M. S., and Rehman, A. (2022): Analytical analysis of the magnetic field, heat generation and absorption, viscous dissipation on couple stress Casson hybrid Nano fluid over a nonlinear stretching surface, *Results in Engineering*, 16, 100601 <https://doi.org/10.1016/j.rineng.2022.100601>
- Ibrahim, S.M.; Lorenzini, G., Vijaya Kumar, P., Raju, C.S.K. (2017): Influence of chemical reaction and heat source on dissipative MHD mixed convection flow of a Casson nanofluid over a nonlinear permeable stretching sheet. *Int. J. Heat Mass Transf.* 111, 346-355. <https://doi.org/10.1016/j.ijheatmasstransfer.2017.03.097>
- Kathyayani G, Lakshmi Devi R. (2019): Numerical Study on The Effect of Linear/Non-Linearly Stretching Sheet with Suction or Injection of MHD Mixed Convection Jeffrey Fluid Flow in A Vertical Stagnation-Point of A Porous Medium in The Presence of Thermal Radiation and Chemical Reaction. *Bulletin of Pure and Applied Sciences Section E – Maths and Stat.* 38E (2), 550-562. <http://dx.doi.org/10.5958/2320-3226.2019.00056.0>

- Khan, M. S., Mei, S., Fernandez-Gamiz, U., Noeiaghdam, S., Khan, A., and Shah, S. A. (2022): Electroviscous Effect of Water-Base Nanofluid Flow between Two Parallel Disks with Suction/Injection Effect. *Mathematics* 10, 956. <https://doi.org/10.3390/math10060956>
- Khan, U., Mahmood, Z., Eldin, S. M., Makhdom, B. M., Fadhl, B. M., and Alshehri, A. (2023): Mathematical analysis of heat and mass transfer on unsteady stagnation point flow of Riga plate with binary chemical reaction and thermal radiation effects. *Heliyon*, 9(3). <https://doi.org.egateway.vit.ac.in/10.1016/j.heliyon.2023.e14472>
- Kumar, A., Tripathi, R., Singh, R. and Sheremet, M. A (2021): Entropy generation on double diffusive MHD Casson nanofluid flow with convective heat transfer and activation energy. *Indian J Phys* 95, 1423–1436. <https://doi.org/10.1007/s12648-020-01800-9>
- Lone, S. A., Shamshuddin, M. D., Shahab, S., Iftikhar, S., Saeed, A., and Galal, A. M. (2023): Computational analysis of MHD driven bioconvective flow of hybrid Casson nanofluid past a permeable exponential stretching sheet with thermophoresis and Brownian motion effects. *Journal of Magnetism and Magnetic Materials*, 580, 170959. <https://doi.org/10.1016/j.jmmm.2023.170959>
- Makhdom, B. M., Mahmood, Z., Fadhl, B. M., Aldhabani, M. S., Khan, U., and Eldin, S. M. (2023): Significance of entropy generation and nanoparticle aggregation on stagnation point flow of nanofluid over stretching sheet with inclined Lorentz force. *Arabian Journal of Chemistry*, 16(6), 104787. <https://doi.org.egateway.vit.ac.in/10.1016/j.arabjc.2023.104787>
- Mirza Naveed Jahangeer Baig , Nadeem Salamat , Faisal Z. Duraihem , Salman Akhtar , Sohail Nadeem , Jehad Alzabut , Salman Saleem. (2023): Exact Analytical Solutions of Stagnation point flow over a Heated stretching cylinder: A phase flow nanofluid model, *Chinese Journal of Physics*. <https://doi.org/10.1016/j.cjph.2023.03.017>
- Pramanik, S. (2014): Casson fluid flow and heat transfer past an exponentially porous stretching surface in presence of thermal radiation. *Ain shams engineering journal*, 5(1), 205-212. <https://doi.org/10.1016/j.asej.2013.05.003>.
- Raizah, Zehba, Saeed, Anwar, Bilal, Muhammad, Galal, Ahmed M. and Bonyah, Ebenezer. (2023): Parametric simulation of stagnation point flow of motile microorganism hybrid nanofluid across a circular cylinder with sinusoidal radius, *Open Physics* 21 (1), 20220205. <https://doi.org/10.1515/phys-2022-0205>
- Raju. S. S. R., Renuka Devi, R. L. V., Asogwa, K. K., Raju, S. S. K., Raju, C. S. K., Kathyayani. G., and Siva Kumar N. (2023): Falkner–Skan slip flow of non-Newtonian fluid over a moving and nonlinearly radiated wedge with variable heat source/sink and viscous dissipation. *International Journal of Modern Physics B*, 2450004. <https://doi.org/10.1142/S0217979224500048>
- Rasool, G., Wakif, A., Wang, X., Shafiq, A., and Chamkha, A. J. (2023): Numerical passive control of alumina nanoparticles in purely aquatic medium featuring EMHD driven non-Darcian nanofluid flow over convective Riga surface. *Alexandria Engineering Journal*, 68, 747-762. <https://doi.org/10.1016/j.aej.2022.12.032>
- Shabnam, Khan, M. S., Mei, S., Fernandez-Gamiz, U., Noeiaghdam, S., and Khan, A. (2022): Numerical Simulation of a Time-Dependent Electroviscous and Hybrid Nanofluid with Darcy-Forchheimer Effect between Squeezing Plates. *Nanomaterials* 12, 876. <https://doi.org/10.3390/nano12050876>
- Shafiq, A., Rasool, G., Wang, X., Chamkha, A. J., and Wakif, A. (2023): Numerical treatment of MHD Al₂O₃–Cu/engine oil-based nanofluid flow in a Darcy–Forchheimer medium: Application of radiative heat and mass transfer laws. *International Journal of Modern Physics B*, 2450129. <https://doi.org/10.1142/S0217979224501297>
- Shah, I. A., Bilal, S., Noeiaghdam, S., Fernandez-Gamiz, U., and Shahzad, H. (2022): Thermosolutal natural convection energy transfer in magnetically influenced casson fluid flow in hexagonal enclosure with fillets, *Results in Engineering* 15, 100584. <https://doi.org/10.1016/j.rineng.2022.100584>
- Sharma, J., Ahammad, N. A., Wakif, A., Shah, N. A., Chung, J. D., and Weera, W. (2023): Solutal effects on thermal sensitivity of casson nanofluids with comparative investigations on Newtonian (water) and non-Newtonian (blood) base liquids. *Alexandria Engineering Journal*, 71, 387-400. <https://doi.org/10.1016/j.aej.2023.03.062>
- Shaw, S., Gorla, R.S.R., Murthy, P.V.S.N. and Ng, C.O. (2009): Pulsatile Casson fluid flow through a stenosed bifurcated artery, *International Journal of Fluid Mechanics Research*, 36, 43-63. <https://doi.org/10.1615/InterJFluidMechRes.v36.i1.30>

Tawade, J. V., Guled, C. N., Noeiaghdam, S., Fernandez-Gamiz, U., Govindan, V., and Balamuralitharan, S. (2022): Effects of thermophoresis and Brownian motion for thermal and chemically reacting Casson nanofluid flow over a linearly stretching sheet Results in Engineering 15, 100448.

<https://doi.org/10.1016/j.rineng.2022.100448>

Thumma, T., Mishra, S.R., Shamshuddin, M. (2019): Effect of Heat Generation and Viscous Dissipation on MHD 3D Casson Nanofluid Flow Past an Impermeable Stretching Sheet. In: Srinivasacharya, D., Reddy, K. (eds) Numerical Heat Transfer and Fluid Flow. Lecture Notes in Mechanical Engineering. Springer, Singapore.

https://doi.org/10.1007/978-981-13-1903-7_66

Tulu, A., and Ibrahim, W. (2020): Spectral relaxation method analysis of Casson nanofluid flow over stretching cylinder with variable thermal conductivity and Cattaneo–Christov heat flux model. Heat Transfer.49 (6), 3433-3455. <https://doi.org/10.1002/htj.21781>

Venkatadri K, Devi TS, Shobha A, Sekhar KR, Rajeswari VR. (2023): Numerical Study of Natural Convection Flow in a Square Porous Enclosure Filled with Casson Viscoelastic Fluid. Contemp. Math. [Internet]. 2023 Jun. 30 [cited 2023 Jul. 24];4(3):379-91.<https://ojs.wiserpub.com/index.php/CM/article/view/2913>

Venkatadri, K., Maheswari, S., Lakshmi, C. V., and Prasad, V. R. (2018): Numerical simulation of lid-driven cavity flow of micropolar fluid. In IOP Conference Series: Materials Science and Engineering (Vol. 402, No. 1, p. 012168). IOP Publishing. Doi: 10.1088/1757-899X/402/1/012168.

Venkata Ramudu, A. C., Anantha Kumar, K., Sugunamma, V., and Sandeep, N. (2020): Heat and mass transfer in MHD Casson nanofluid flow past a stretching sheet with thermophoresis and Brownian motion. Heat Transfer, 49(8), 5020–5037. <https://doi.org/10.1002/htj.21865>

Vijay, N., and Sharma, K. (2023): Dynamics of stagnation point flow of Maxwell nanofluid with combined heat and mass transfer effects: A numerical investigation. International Communications in Heat and Mass Transfer, 141, 106545. <https://doi-org.egateway.vit.ac.in/10.1016/j.icheatmasstransfer.2022.106545>

Wakif, A., Abderrahmane, A., Guedri, K., Bouallegue, B., Kaewthongrach, R., Kaewmesri, P., and Jirawattanapanit, A. (2022): Importance of exponentially falling variability in heat generation on chemically reactive von kármán nanofluid flows subjected to a radial magnetic field and controlled locally by zero mass flux and convective heating conditions: a differential quadrature analysis. Frontiers in Physics, 10, 988275. <https://doi.org/10.3389/fphy.2022.988275>

Wakif, A. (2023): Numerical inspection of two-dimensional MHD mixed bioconvective flows of radiating Maxwell nanofluids nearby a convectively heated vertical surface. Waves in Random and Complex Media, 1-22. <https://doi.org/10.1080/17455030.2023.2179853>

Zhang, K., Shah, N. A., Alshehri, M., Alkarni, S., Wakif, A., and Eldin, S. M. (2023) Water thermal enhancement in a porous medium via a suspension of hybrid nanoparticles: MHD mixed convective Falkner's-Skan flow case study. Case Studies in Thermal Engineering, 47, 103062. <https://doi.org/10.1016/j.csite.2023.103062>